



THE UNIVERSITY *of* EDINBURGH

Edinburgh Research Explorer

Pressure-induced amorphization and existence of molecular and polymeric amorphous forms in dense SO₂

Citation for published version:

Zhang, H, Troth, O, Liu, X-D, Bini, R, Gregoryanz, E, Dalladay-Simpson, P, De Panfilis, S, Santoro, M, Gorelli, FA & Martonak, R 2020, 'Pressure-induced amorphization and existence of molecular and polymeric amorphous forms in dense SO₂', *Proceedings of the National Academy of Sciences of the United States of America*. <https://doi.org/10.1073/pnas.1917749117>

Digital Object Identifier (DOI):

[10.1073/pnas.1917749117](https://doi.org/10.1073/pnas.1917749117)

Link:

[Link to publication record in Edinburgh Research Explorer](#)

Document Version:

Peer reviewed version

Published In:

Proceedings of the National Academy of Sciences of the United States of America

General rights

Copyright for the publications made accessible via the Edinburgh Research Explorer is retained by the author(s) and / or other copyright owners and it is a condition of accessing these publications that users recognise and abide by the legal requirements associated with these rights.

Take down policy

The University of Edinburgh has made every reasonable effort to ensure that Edinburgh Research Explorer content complies with UK legislation. If you believe that the public display of this file breaches copyright please contact openaccess@ed.ac.uk providing details, and we will remove access to the work immediately and investigate your claim.



Pressure-induced amorphization and existence of molecular and polymeric amorphous forms in dense SO₂

Huichao Zhang^{a,b}, Ondrej Tóth^c, Xiao-Di Liu^{a,2}, Roberto Bini^d, Eugene Gregoryanz^{a,e,f}, Philip Dalladay-Simpson^f, Simone De Panfilis^g, Mario Santoro^{a,h,2}, Federico Aiace Gorelli^{a,h,2}, and Roman Martoňák^{c,2}

^aKey Laboratory of Materials Physics, Institute of Solid State Physics, Chinese Academy of Sciences, Hefei, 230031, China; ^bUniversity of Science and Technology of China, Hefei 230026, China; ^cDepartment of Experimental Physics, Comenius University, Mlynská Dolina F1, 842 48 Bratislava, Slovakia; ^dDepartment of Chemistry Univ Florence and European Laboratory for non Linear Spectroscopy (LENS), via N. Carrara 1, 50019 Sesto Fiorentino, Italy; ^eSchool of Physics and Astronomy and Centre for Science at Extreme Conditions, University of Edinburgh, Edinburgh EH9 3JZ, UK; ^fCenter for High Pressure Science Technology Advanced Research, 1690 Cailun Road, Shanghai, 201203, China; ^gCentre for Life Nano Science, Istituto Italiano di Tecnologia, viale Regina Elena 291, 00161 Rome, Italy; ^hIstituto Nazionale di Ottica (CNR-INO) and European Laboratory for non Linear Spectroscopy (LENS), via N. Carrara 1, 50019 Sesto Fiorentino, Italy

This manuscript was compiled on January 17, 2020

We report here the pressure-induced amorphization and reversible structural transformation between two amorphous forms of SO₂: molecular-amorphous and polymeric-amorphous, with the transition found at 26 GPa over a broad temperature regime, 77 - 300 K. The transformation was observed by both Raman spectroscopy and x-ray diffraction in a diamond anvil cell. The results were corroborated by *ab initio* molecular dynamics simulations, where both forward and reverse transitions were detected, opening a window to detailed analysis of the respective local structures. The high-pressure polymeric-amorphous form was found to consist mainly of disordered polymeric chains made of 3-coordinated sulfur atoms connected via oxygen atoms, with few residual intact molecules. This study provides an example of polymorphism in a system consisting of simple molecules with multiple bonds.

polyamorphism | sulfur dioxide | high pressure | polymeric form

Polyamorphism is the counterpart of polymorphism observed in crystalline solids. It is characterized by the existence of two or more disordered forms, either amorphous or liquid, differing in local structural order whilst preserving the stoichiometry. This phenomenon is often also accompanied by changes in coordination and density (1, 2) (for recent reviews see Refs. (3, 4)). Transformations between these different amorphous forms can be driven by pressure and temperature. While in the case of crystalline polymorphs the structural transitions are often (at least in principle) of first order and sharp, transitions in amorphous systems occur among isotropic forms and are more likely to be continuous. This is related to the absence of constraints prescribed by lattice periodicity, allowing for a gradual transformation between very different forms.

The first and perhaps most celebrated example of polyamorphic behavior was discovered in water ice by Mishima in 1984 (5, 6), observing that compression of ice I_h at 77 K induced a transformation to an amorphous state. Through specific compression/decompression/heating protocols, at least two different forms of amorphous water ice were identified, known as low-density amorphous (LDA) and high-density amorphous (HDA) ices. The local structural order in the HDA and LDA ices differs by the presence of nonbonded water molecules in the first coordination shell of the former, resulting in the two forms having substantially different density. The existence of two amorphous forms of water ice was suggested to be related to existence of liquid-liquid transition and a second critical

point of water (7).

Since, similar phenomena have also been observed in other systems such as Si (8), SiO₂ (9–11), GeO₂ (12), where the polyamorphism is related to a change from tetrahedral to octahedral coordination at high pressure. Other examples where pressure induces changes in simple molecular systems include amorphous S (13) and liquid S (14) (for more examples and review see Refs. (3, 4)). Dramatic structural changes leading to amorphization have been observed upon compression of molecular crystals where multiple bonds are present. It is well known that pressure can destabilize multiple bonds in molecules in favour of extended polymeric networks with a higher coordination. Due to the associated strong kinetic effects, creation of amorphous phases are often observed, especially, when compression is performed at low temperatures. Amorphization of molecular crystals at high pressure have been observed in the famous examples of nitrogen (15, 16),

Significance Statement

Some substances are known to exist in several different structurally disordered solid states and transform between them similarly to structural phase transitions between crystalline polymorphs. This interesting and yet not fully understood phenomenon is called polyamorphism and notable examples include water, SiO₂, Si, etc. Here we present a new example of such behavior in a simple molecular substance, SO₂. By using experimental high-pressure techniques we observe a reversible transition between different amorphous states around 26 GPa. Experimental results are well supported by *ab initio* simulations, which identify the high-pressure amorphous form as non-molecular, polymeric one consisting of intertwined chains. Our findings contribute to the fundamental understanding of structure of disordered matter as well as high-pressure behaviour of simple archetypal molecules.

H.C.Z. performed the experiments and contributed to the data analysis. O.T. performed simulations, analyzed the data and wrote the paper. X.D.L., R.B. and E.G. contributed to the discussion of results and wrote the paper. P.D.S. conducted the experiments and wrote the paper. X.D.L., P.D.S. and E.G. contributed materials/analysis tools. S.D.P. analyzed the data, contributed to the discussion of the results and wrote the paper. M.S. and F.A.G. designed the research, contributed to plan the experiments, to the data analysis and wrote the paper. R.M. designed the research, contributed to the analysis and discussion of results and wrote the paper.

The authors declare no conflict of interest.

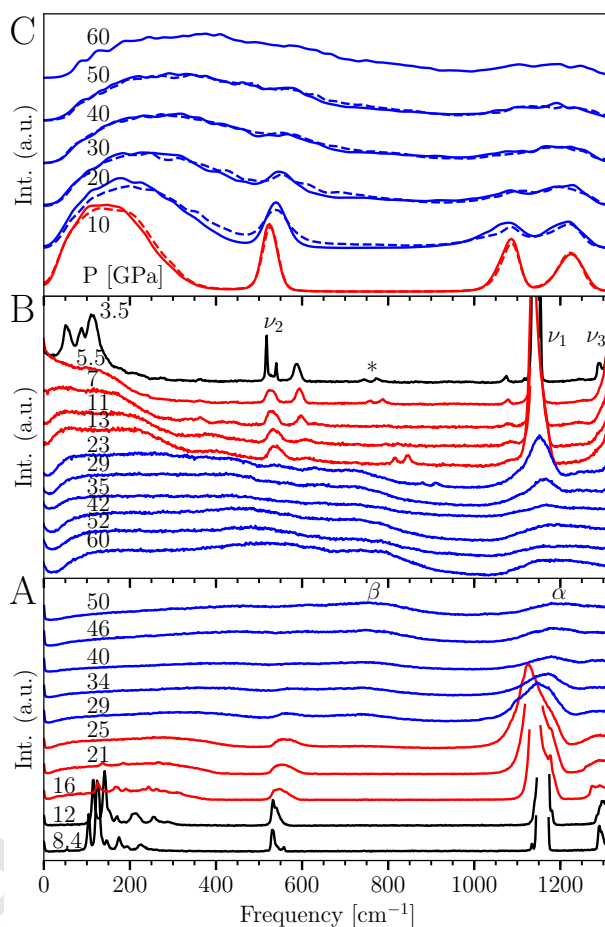
²To whom correspondence may be addressed. Email: gorelli@lens.unifi.it, xiaodi@issp.ac.cn, santoro@lens.unifi.it or martonak@imph.uniba.sk

46 carbon dioxide (17, 18) and benzene (19–21). In nitrogen, the
 47 strong triple bond of the molecule breaks under high pressures
 48 giving rise to a single-bonded network. Whilst in carbon
 49 dioxide, the double bond becomes unstable and carbon co-
 50 ordination increases to 3 and 4. In the case of benzene the
 51 aromatic ring opens and a network of hydrogenated carbons
 52 with single bonds is formed. The parent crystalline states
 53 of these amorphous materials have been discovered both in
 54 nitrogen (22, 23) and in carbon dioxide (24, 25) after high
 55 temperature annealing obtained by means of laser heating.

56 Sulphur dioxide is an important molecule in chemistry,
 57 serves a significant role in industrial applications, and has
 58 been attributed to atmospheric and geological processes. Un-
 59 like CO₂, the SO₂ molecule is bent, described by two resonant
 60 structures with one single and one double bond(26, 27). The
 61 crystalline forms of SO₂ have been previously experimentally
 62 studied at pressures up to 32 GPa by Song et al.(28). Here,
 63 we present a combined experimental and computational study
 64 of SO₂ up to pressures of 60 GPa and over a broad tempera-
 65 ture regime. Observations via Raman spectroscopy and X-ray
 66 diffraction, well supported by *ab initio* simulations, provide a
 67 detailed description on the atomistic level of the transforma-
 68 tions under compression/decompression cycles. These findings
 69 give evidence of a hitherto unobserved example of polyamor-
 70 phism related to a reversible transformation between molecular
 71 and polymeric amorphous forms of SO₂.

72 In Fig. 1, we present a selection of Raman spectra measured
 73 upon increasing pressure up to 60 GPa, at 77 K (panel A), as
 74 well as subsequent decompression back to ambient pressure at
 75 room temperature (panel B). Similar experiments for compres-
 76 sions at 210 K were also conducted and reported in Fig. S1
 77 Supp. Mat. We find in general, an agreement between our
 78 Raman measurements of solid molecular SO₂ under pressure
 79 and those reported previously (28). However, the dramatic
 80 spectral changes at low temperatures were not observed pre-
 81 viously as pressures were limited to only 22 GPa (28). From
 82 these datasets, what is readily evident is the progression from
 83 sharp molecular peaks of SO₂, i. e. ν_1 1050-1220 cm⁻¹, ν_3
 84 1240-1320 cm⁻¹ and ν_2 520-600 cm⁻¹, to much broader, weaker
 85 peaks upon compression. In addition, new broad and weak
 86 bands appear at different frequencies, characteristics which
 87 are compatible with pressure-induced amorphization together
 88 with major changes in the local structure. Further, the well-
 89 defined molecular peaks of SO₂ are recovered upon decreasing
 90 pressure, while the new broad bands disappear, demonstrating
 91 that these changes are indeed reversible and are therefore
 92 incompatible with any irreversible processes, such as chemical
 93 decomposition (SO₂ → S + O₂).

94 Taking a detailed analysis of the spectra, we can shed
 95 light on a number of remarkable features. We find that the
 96 numerous sharp lattice peaks, observed below 300-400 cm⁻¹,
 97 weaken above 16 GPa until they become undetectable above
 98 21 GPa at 77 K (Fig. 1 A) or above 10 GPa at 210 K (Fig. S1
 99 Supp. Mat.), and instead are replaced by a new broad band
 100 in the same spectral region. However, at higher frequencies,
 101 under the same conditions, we do not observe any additional
 102 peaks other than the molecular peaks, ν_1 , ν_2 , and ν_3 , of SO₂
 103 up to 25 GPa. The linewidth of the crystal peaks severely
 104 increases upon growing pressure while the intensity decreases
 105 substantially. These spectral changes are highly indicative that
 106 upon cold compression above 10-15 GPa, crystalline molecular



107 **Fig. 1.** Vibrational spectra of solid SO₂. Panels A and B: selected Raman spectra of
 108 an SO₂ sample measured upon increasing pressure at 77 K (A) and decreasing pres-
 109 sure at room temperature (B). During compression, the initially sharp molecular
 110 peaks of SO₂, ν_1 , ν_2 , and ν_3 , broaden and become very weak while new broad and weak
 111 bands appear at different frequencies, indicating pressure-induced amorphization to-
 112 gether with changes in the local structure. Upon decompression, the sharp molecular
 113 peaks of SO₂, ν_1 , ν_2 , and ν_3 , are recovered while the new broad bands disappear at
 114 the same time, showing that amorphization and overall changes in the local structure
 115 are reversible. Panel C: evolution of vibrational density of states (VDOS) from *ab*
 116 *initio* MD simulations along compression (solid lines) and decompression (dashed
 117 lines). Color represents structural state of the system: black - molecular crystal, red -
 118 molecular amorphous and blue - polymeric amorphous. Star in panel B marks ruby
 119 peaks.

120 SO₂ undergoes a structural transformation into an amorphous
 121 form whilst preserving its molecularly, i. e. consisting of SO₂
 122 molecular units. Amorphization could have been enhanced by
 the shear stress, which is in turn related to the deformation of
 the gasket hole. This is supported also by our DFT calculations
 (see section on simulation results). Upon further compression,
 above 22-25 GPa, additional and significant modifications
 to the Raman signature are observed, the ν_2 and ν_3 peaks
 progressively diminish and are barely observable above 30-34
 GPa. Conversely, the strongest Raman excitation of SO₂,
 ν_1 (1170-1200 cm⁻¹ (Fig. 1 A)), is visible to the maximum
 pressures of 50-60 GPa (see also Fig. 1 B), albeit comparatively
 weaker. The ν_1 band peak is found to merge with an altogether
 new weak and broad peak centred at 1220-1230 cm⁻¹, denoted
 as α in Fig. 1 A. In addition to emergence of the α -peak,
 another new and broad band appears, at 600-1000 cm⁻¹ with

123 a high frequency edge at around 900 cm^{-1} , which we call β .
 124 Both bands α and β appear to be of non-molecular origin,
 125 which suggests that the emergence of these excitations signals
 126 that amorphous-molecular SO_2 undergoes a transformation
 127 into a non-molecular/extended amorphous form.

128 Comparison with the pressure-induced molecular to
 129 amorphous-non-molecular transformation in CO_2 (17, 18, 25)
 130 can help to interpret the transformation observed here in SO_2 ,
 131 as it bears similarities. Carbonia, the non-molecular amorphous
 132 CO_2 , has been shown to be made of a mixture of C
 133 in a 3-fold and 4-fold oxygen coordination in similar propor-
 134 tions. The 3-fold coordinated C sites are uniquely identified
 135 by C=O stretching peaks in the Raman and the IR spectrum,
 136 $1900\text{-}2000\text{ cm}^{-1}$ at $50\text{-}60\text{ GPa}$, which roughly corresponds to
 137 the average value, $\nu(\text{stretch CO}_2)$, between the symmetric
 138 and the antisymmetric stretching modes of molecular CO_2 .
 139 However, when considering the full Raman and IR spectra, the
 140 single C-O bond stretching and deformation modes ascribed
 141 to both 3-fold and 4-fold coordinated C sites, form a broad
 142 spectral distribution extending over $500\text{-}1500\text{ cm}^{-1}$, approxi-
 143 mately $0.26\text{-}0.77$ of the average $\nu(\text{stretch CO}_2)$. Consequently,
 144 in the case of SO_2 , the aforementioned peak, α , is roughly the
 145 average frequency of the two molecular stretching modes, and
 146 can therefore be attributed to the S=O stretching modes for
 147 non-molecular/extended SO_2 with S in 3-fold coordination by
 148 O. In addition, in the frequency range given by $0.26\text{-}0.77$ of
 149 α , $320\text{-}940\text{ cm}^{-1}$, we observe the previously described band
 150 β . Therefore, again in accordance with the CO_2 analogue,
 151 the β band can be attributed to single S-O bond stretching
 152 and deformation modes in the non-molecular/extended SO_2 .
 153 A discrepancy of using carbonia as an analogue however is
 154 that the 4-fold oxygen coordination is absent in SO_2 , in ac-
 155 cordance with our DFT simulations (discussed later). We
 156 do however also have a two component system, considering
 157 that the ν_1 peak for molecular SO_2 is still present at the
 158 highest pressures, although weak. Therefore, inferring that
 159 the overall non-molecular/extended SO_2 consists of a mixture
 160 of trace 2-fold S sites, still molecular in nature, in a bulk
 161 of non-molecular 3-fold coordinated S sites. An alternative
 162 possibility compatible with experimental data would be that
 163 molecular parts of the sample with 2-fold coordinated S and
 164 non-molecular parts with S in higher coordination are phase
 165 separated on a macroscopic/mesoscopic scale.

166 On decompression, the spectral changes and transforma-
 167 tions identified previously on compression are reverted, demon-
 168 strated in Fig. 1 B. However, a minor hysteresis is observed,
 169 attributed to the kinetically limited structural changes. We
 170 observe that when the sample is decompressed below $30\text{-}25$
 171 GPa, both the α peak and β band disappear, whilst the
 172 well-defined molecular peaks ν_1 , ν_2 , and ν_3 emerge suddenly.
 173 Further, in the low frequency/lattice region below 350 cm^{-1} a
 174 diffuse, liquid-like band clearly develops, with no additional
 175 substantial changes down to about 5 GPa . These changes
 176 demonstrate again a change in the amorphous structure, re-
 177 covering molecular SO_2 units at $25\text{-}5\text{ GPa}$ on decompression.
 178 This molecular-amorphous phase is then found to further trans-
 179 form into a crystalline molecular SO_2 structure below 5 GPa ,
 180 indicated by the sharp lattice mode peaks observed below
 181 this pressure and crystalline x-ray diffraction (discussed later).
 182 Interestingly, an additional peak is found below 20 GPa at
 183 around 600 cm^{-1} which was also observed in a previous study,

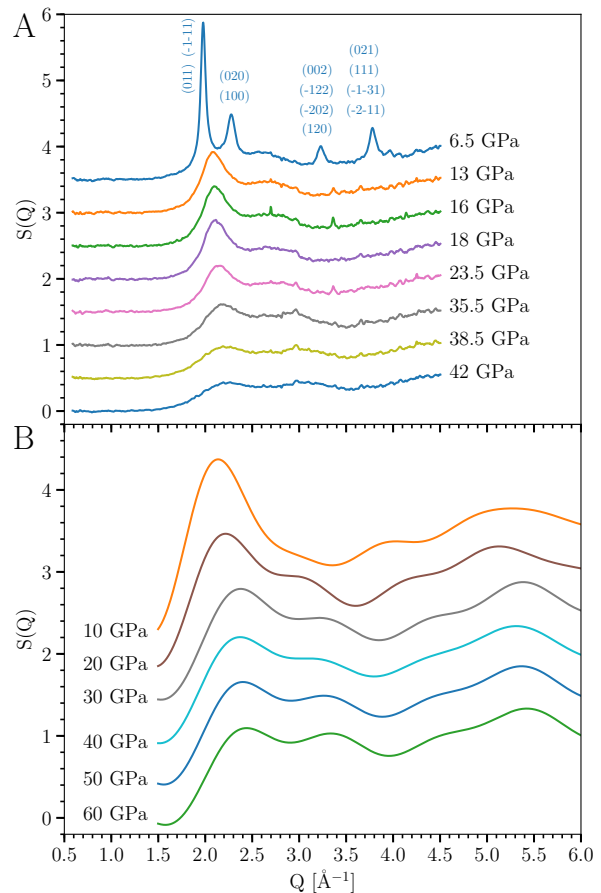


Fig. 2. Static structure factor of solid SO_2 under pressure. Panel A: experimental $S(Q)$ measured along a room temperature decompression run, panel B: $S(Q)$ computed from simulations at 300 K during decompression (the graph computed from simulation of compression is in Supp. Mat. Fig. S2. Region of $S(Q)$ beyond 4.5 \AA^{-1} in A is inaccessible because of limited angle in experiment, while the region below 1.5 \AA^{-1} in B is not reliable because of limited RDF range, resulting from the simulation supercell size of 14 \AA . The Bragg peaks have been indexed on the basis of a $Aea2$ space group with $a=5.5430\text{ \AA}$, $b=5.4011\text{ \AA}$, $c=5.5356\text{ \AA}$ as obtained from simulations (see also Fig. S11 in Supp. Mat.).

184 where it was attributed to the formation of molecular clusters
 185 (28). The reversible transformations of SO_2 to molecular and
 186 non-molecular amorphous forms again parallel the similar case
 187 of CO_2 (17, 18, 25), and at odds with the cases of aromatic
 188 molecules, where instead amorphous non-molecular forms ob-
 189 tained at high pressures are recoverable to ambient conditions
 190 (19–21, 29, 30).

191 The non-crystalline nature of SO_2 at high pressure has also
 192 been assessed by x-ray diffraction, and the evolution of the
 193 static structure factor upon room temperature decompression
 194 of sample compressed at low temperature is shown in Fig. 2 A.
 195 The static structure factor has been obtained by the empty cell
 196 subtraction, taking into account the form factors of oxygen and
 197 sulfur as well as the Compton contribution from the sample,
 198 following a procedure described elsewhere (31). In general, it
 199 is found that at the highest pressures the two peaks at about
 200 2.2 and 3 \AA^{-1} are of similar intensity, while on decompression
 201 the first peak significantly increases with respect to the second
 202 one which at the same time moves to lower Q . Critically, in

203 comparison between patterns measured at 35.5 and 23.5 GPa,
 204 there is a clear change of the static structure factor. The first
 205 contribution, centred at 2.2 \AA^{-1} , becomes more prominent and
 206 sharpens markedly, whilst the second has a more subtle loss of
 207 intensity. These changes, corresponding to the transformation
 208 from an extended amorphous to a molecular amorphous form,
 209 are in strong agreement with the Raman results outlined
 210 previously.

211 In summary, we have observed two distinct structural trans-
 212 formations. At lower pressures, the transformation from a
 213 molecular crystal to a molecular, van der Waals type, amor-
 214 phous solid, with no changes in the molecular unit and to a
 215 non-molecular/extended state on further compression. Inter-
 216 estingly, a substantial effect of temperature is observed for the
 217 former transformation, despite the expected energy barrier to
 218 be comparatively small. For example, instead of an expected
 219 isobaric phase line, the transformation occurs at 5 GPa lower
 220 pressures at 210 K compared with 77 K isotherm. Conversely,
 221 the second transformation, to a non-molecular/extended amor-
 222 phous state, is a chemically reconstructive one, and therefore
 223 would logically have a higher associated energy barrier and
 224 consequently a stronger temperature dependence. Instead, this
 225 transformation is observed at roughly the same pressures for
 226 both isotherms studied, 77 K and 210 K, at around 25-30 GPa,
 227 counterintuitively suggesting that the barrier for polymeriza-
 228 tion is small in relation to the initial molecular amorphisation.
 229 We note that this is quite different from the case of CO_2 and
 230 N_2 , where a much stronger hysteresis is reported (23–25).

231 In order to obtain a better understanding of the processes
 232 on the atomistic level, we performed *ab initio* MD simulations
 233 following a pressure path akin to the experiment. We first
 234 performed a test in order to check whether applying shear stress
 235 to a perfect *Aea2* molecular crystal at low pressure might result
 236 in amorphous molecular structure as observed in experiments.
 237 We gradually induced shear strain by deforming the γ angle of
 238 the supercell by up to 30° and observed transformation into
 239 a disordered molecular form, confirming the experimentally
 240 observed amorphization.

241 The full simulation protocol is shown in Fig. S3 in Supp.
 242 Mat. In order to start the compression from a well-defined
 243 amorphous molecular structure, we melted a perfect *Aea2*
 244 molecular crystal (32) in a $3 \times 3 \times 3$ supercell (108 SO_2
 245 molecules, equivalent to a 324 atom unit cell) by heating
 246 at $P = 0$ GPa to 600 K. Through subsequent cooling to 0
 247 K, we prepared the amorphous structure, which served as an
 248 initial configuration for further simulations. Following the
 249 experimental pathway, we performed a gradual compression
 250 to 60 GPa and subsequent decompression to 10 GPa (in 10
 251 GPa steps) at 300 K in order to accelerate the structural
 252 transformations (both on compression and decompression). In-
 253 terestingly, at this temperature we observed some diffusion of
 254 molecules in the molecular phase, suggesting that the sample
 255 might possibly be in metastable liquid regime.

256 Analysis of the partial radial distribution functions (RDFs)
 257 (Fig. 3), obtained from simulations, can provide a more detailed
 258 description of the observed transformations on an atomistic
 259 level. The RDFs clearly indicate the reversible amorphous
 260 to amorphous transformation, corresponding to the S in 2-
 261 to 3-fold O coordination change, providing further evidence
 262 for the experimentally observed phases and their associated
 263 reversibility. Upon compression of the initial molecular amor-

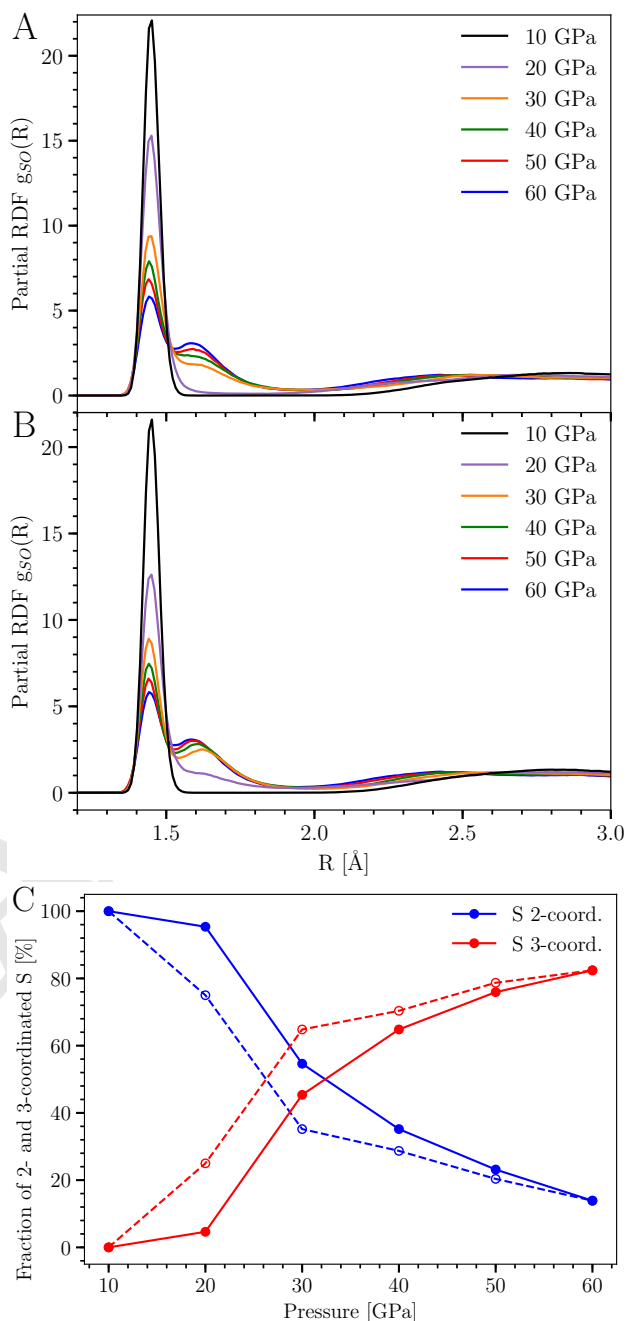


Fig. 3. Partial S-O radial distribution function (RDF) and concentration of sulfur coordination states. Panel A: RDF during compression, panel B: RDF during decompression and panel C: fraction of 2- and 3-coordinated S atoms during compression (solid line) and decompression (dashed line). Coordination number was determined within the cutoff of 1.92 Å.

264 phous sample to 10 GPa at 300 K, SO_2 retains its molecular
 265 units. Evidenced in Fig. 3 A, the peak at 1.44 Å, correspond-
 266 ing to the double bond, is sharp and well separated from the
 267 next neighbor at 2.5-3.0 Å and the coordination number of S
 268 atoms with respect to O atoms is 2. Upon compression to 20
 269 GPa modifications in the RDF are observed, and at 30 GPa
 270 there is a substantial change, the first peak becomes weaker
 271 whilst a new peak at slightly longer distance, 1.6 Å, appears.
 272 These changes indicate that some of S=O double bonds are

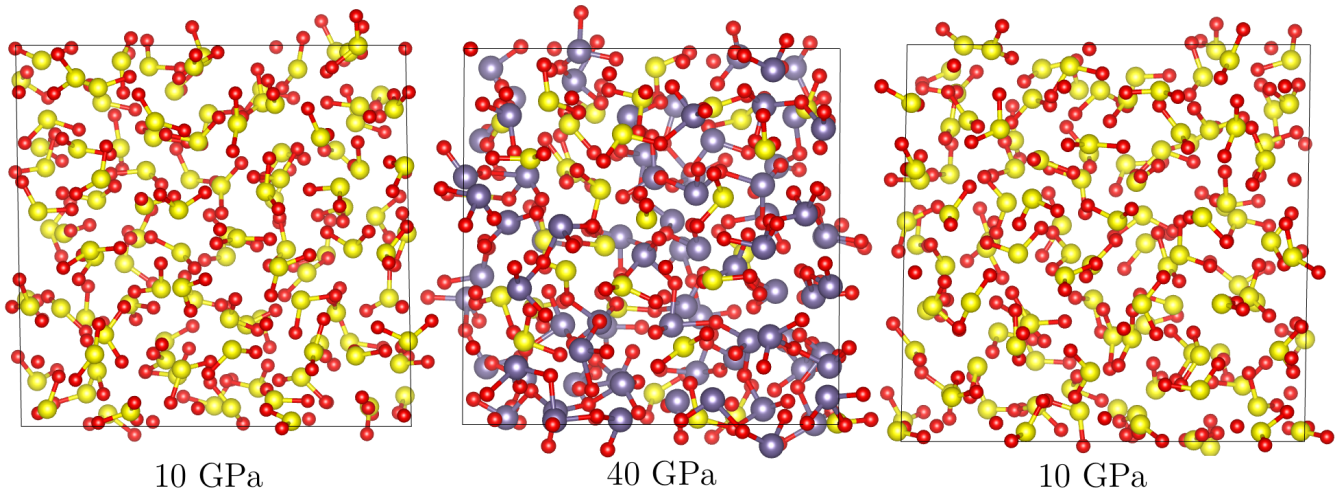


Fig. 4. Snapshots of the simulated sample at different pressures. Left panel: the beginning of compression at 10 GPa where sample consists only of SO_2 molecules. Middle panel: structure during compression at 40 GPa with S atoms colored by coordination: 2-yellow (molecule) and 3-gray (polymeric chains). Right panel: structure after decompression to 10 GPa reverted from polymeric back to molecular. Simulation supercells are not to scale.

broken and replaced by single ones. In the same pressure regime, 3-coordinated S-atoms appear with 2 single S-O bonds and one S=O double bond, forming polymeric chains (see snapshots shown in Fig. 4). On further compression, the first peak is found to progressively diminish in intensity whilst the second is enhanced, resulting in 82 % of S atoms to be in a 3-fold oxygen coordination at 60 GPa. On decompression (see Fig. 3 B), akin to experimental observations, we observed the reverse evolution, further demonstrated by the pressure dependence of the number of 2- and 3-coordinated S atoms in Fig. 3 C. Additionally, at 10 GPa the previously identified polymeric chains observed on compression disappear entirely (see Fig. 4), and the system reverts back to its initial molecular amorphous state. The strong agreement between experiment and simulations, means that insights from the MD-calculations can identify the experimental observations as forward and backward transitions between molecular and polymeric amorphous forms of SO_2 . The dependence of the coordination number of S atoms on pressure (Fig. 3 C) exhibits some hysteresis, which suggests that the transition might have a weakly first-order character. The pressure dependence of density upon compression and decompression, shown in Fig. S4 (Supp. Mat.) shows a very small hysteresis and does not exhibit any particular features across the structural transformation. We performed a similar compression simulation also at 500 K and found the polymerization to start at 30 GPa, suggesting that the transition is shifted to higher pressure upon increasing temperature.

Above 20 GPa, the calculated static structure factor, $S(Q)$, shows important changes upon compression (Fig. S2 Supp. Mat.). The intensity of the first diffraction peak at about 2.2 \AA^{-1} drops, while a new peak appears, around 3 \AA^{-1} , which grows with increasing pressure. At 60 GPa, the height of both peaks becomes similar, reflecting XRD patterns above 35.5 GPa in Fig. 2 A. All changes are found to be reversible upon decompression, albeit with a small hysteresis, and the calculated structure factor agrees very well with the experimental one (Fig. 2). Simulations allow us to decompose the total $S(Q)$ into contributions from atomic pairs (Figs. S5 Supp. Mat.) The first peak, around 2.2 \AA^{-1} , originates mainly from

non-bonded S \cdots S pairs, while the weaker second peak, at 3 \AA^{-1} , comes from O \cdots O and finally the broad peak, around 5 \AA^{-1} , is mainly due to the S-O pairs. It is clear that the loss of the first peak of total $S(Q)$ is a consequence of changes in the S-O contribution, which exhibits a pronounced drop above 20 GPa (Fig. S5 Supp. Mat.). Therefore, the observed evolution of $S(Q)$ can directly reflect changes of the distance of S-O neighbors upon polymerization.

On compression, comparing the vibrational spectra from simulations (Fig. 1 C) with experimental Raman spectra (Fig. 1 A), we observe qualitatively similar evolution. Above 20 GPa the distinct ν_2 peak at 550 cm^{-1} progressively disappears whilst the $400 - 500$ and $600 - 900 \text{ cm}^{-1}$ regions become enhanced. Meanwhile, the two molecular peaks, ν_1 around 1100 cm^{-1} and ν_3 above 1200 cm^{-1} gradually merge into a single broad peak around 1200 cm^{-1} , again in agreement with experiments (Fig. 1 A). The evolution of the peaks can be understood from the projected VDOS, allowing decomposition of the total VDOS into contributions from structurally distinct S and O atoms (Fig. S6 Supp. Mat.). Both S and O atoms can be either in molecules or in polymeric chains. Moreover, O atoms in polymeric chains are either at a bridging position between two S atoms (S-O-S) or at terminal position, doubly bonded to S atoms (S=O). The evolution of the total VDOS clearly reflects the gradual conversion of molecules into polymeric chains. Again, upon decompression the reverse evolution is observed, in agreement with experiment (Fig. 1 B).

In order to understand the origin of the two amorphous phases it is useful to discuss their underlying crystalline counterparts. SO_2 forms at ambient pressure and low temperature below 201 K, an $Aea2$ molecular crystal (32). Instead, its analogue SeO_2 forms at ambient pressure a $P4_2/mbc$ polymeric crystal consisting of chains (mineral Downeyite (33)). The possible existence of polymeric SO_2 (polysulfite) was studied in Refs. (34, 35) where energies of various oligomers were calculated. Additionally, in Ref. (35) a crystal structure with infinite polymeric chains was studied obtained by substituting Se atoms in Downeyite by S atoms. It was concluded that polymeric SO_2 is energetically higher than its molecular form and it was proposed that the polymer could be stabilized at

high pressure. This can be understood by applying the well-known pressure-homology rule(36), (37), (38) stating that light elements behave at high pressure like more heavy elements from the same group at lower pressures.

The structure of polymeric phases of SO_2 has not been, to our knowledge, determined experimentally. In order to check its possible existence at high pressure we performed a structural search of crystalline phases of SO_2 employing evolutionary approach (details are described in Methods). We show here the main results of our search. The enthalpy vs. pressure graph for low-enthalpy phases is shown in Supp. Mat. Fig. S7. At zero pressure we found the molecular crystal structure with space group $Aea2$, in agreement with experiment(32). Upon increasing pressure we found another molecular crystal structure $P2_1/c$ which becomes stable above 1 GPa. Besides this structure there are two low-lying metastable molecular structures Pc , and Cc , which around 11 GPa transform into different molecular forms with space groups $Pmc2_1$ and $Ama2$, respectively and become stable (both have very similar enthalpies) with respect to the $P2_1/c$ one. Upon further compression they transform into polymeric structures (all structures are shown in Supp. Mat. Fig. S8 and cif files of the $Pmc2_1$ and $Ama2$ structures are included in Supp. Mat.). Both polymeric structures still have very similar enthalpy and conformation of chains and differ only in chain stacking. The mechanism of polymerization is illustrated in Fig. S9 Supp. Mat. showing the pressure evolution of bond-lengths upon compression. A similar polymerization mechanism is likely to apply also in the amorphous phase when molecules of suitable orientation approach each other. Both polymeric structures have the same conformation of chains as SeO_2 downeyite but the stacking of chains is different. The stable polymeric structure has at 20 GPa bond length of 1.46 Å between S atom and terminal oxygen (S=O) and 1.65 Å between S atom and bridging oxygen (S-O), similar to the peak positions of S-O RDF (Fig. 3). The sulphur atom in the chain is surrounded by three oxygen atoms in roughly trigonal pyramid coordination (at 20 GPa bond angle O-S-O is 90° and O=S-O is 100°) suggesting presence of sp^3 hybridization (see also Ref.(35) where it was suggested that the dimerization of SO_2 is related to $sp^2 \rightarrow sp^3$ rehybridization). In order to quantitatively assess the bond order of S O bonds in molecular and polymeric SO_2 we employed the DDEC6 atomic population analysis method(39). We found a bond order of 2.12 in molecule and 2.14 and 1.15 for S=O and S-O bonds in the polymeric phase. In Fig. S10 Supp. Mat. we show the e-DOS including projections on s and p orbitals for the crystalline molecular and polymeric phase (no d -orbital participation was found). We also note that the diffraction pattern of the recrystallized phase upon decompression to 6.5 GPa (Fig.2 A) shows a strong similarity with the diffraction pattern of the molecular phase $Aea2$ at the same pressure (for comparison see Fig. S11 Supp. Mat.). This provides an additional evidence that the system after the compression/decompression cycle returns to its parent state.

To assess quantitatively the effects of structural disorder, we calculated the enthalpy of the amorphous phase (relaxed to $T = 0$) and found it at 10 GPa to be about 0.26 eV/formula unit above the crystalline phases (it is shown in Fig. S7 in Supp. Mat.). We note that because of the short time scale available in the ab initio MD simulations (of the order of 10 ps) the amorphous structure might not be fully relaxed

structurally. We also determined with our DFT simulations the electronic properties of the a- SO_2 phase. The system does not metalize up to 60 GPa, with band gap of at least 0.6 eV in PBE approximation.

Conclusions and outlook. We observed a pressure-induced amorphization and a reversible structural transition between molecular and polymeric amorphous forms of SO_2 at pressures around 26 GPa. The transition has small hysteresis pointing to the fact that the associated kinetic barriers are low. The lower pressure of the transition between molecular and polymeric amorphous forms, as well as the back transformation, is qualitatively facilitated by the molecular polarity. This, supported by the high density attainable under pressure, drives the intermolecular interaction and lowers the activation energy of the transformation. To our knowledge this kind of transition was not yet observed and provides a new example of structural transition between disordered non-equilibrium states of solid matter. Unlike in a- CO_2 , where polymeric a-carbonia contains 3- as well as 4-coordinated C atoms, here the molecular form converts into polymeric form with only 3-coordinated S atoms. It will be of interest to study whether the two amorphous states continue to exist also in liquid state, either in stable or metastable (undercooled) region. Further experimental and theoretical work is necessary to accurately map the solid and liquid regions and uncover further details of the phase diagram of SO_2 .

Materials and Methods

Experimental methodology. The SO_2 gas was loaded into the DAC by means of cryogenic loading; the gas was condensed between one diamond anvil and the gasket placed on the other diamond of a DAC which was opened by few mm and cooled to liquid nitrogen temperature inside a sealed glove box purged with nitrogen to avoid moisture condensation. We performed Raman spectroscopy using a state of the art confocal Raman microscope with 15 and 2 micron of axial and transverse resolution respectively. The spectrometer consisted of a Spectra Pro 750 mm monochromator, equipped with Pixis Princeton Instrument CCD detector. Bragg grate filters were used to attenuate the laser light and spatial filtering of the collected light to obtain high quality spectra down to 7 cm^{-1} with minimal background from the diamond anvils and strong signal from the sample. The laser beam was expanded and cleaned by a Band Pass Filter. We used a Laser Torus at 660 nm with 10 mW of power and Laser Ventus at 532 nm with 0.5 mW of power to check for the presence of eventual fluorescence bands in the spectrum. We generally used a 300 gr/mm grating as the spectral features were getting very broad and weak with pressure. The pressure was determined by the fluorescence of a small ruby placed in the sample or from the diamond stressed edge which we detect with high accuracy thanks to the excellent spatial resolution of the setup. The XRD measurements were made at Petra (proposal ID: I-20181128) using monochromatic X-ray beam with 42.7 keV energy ($\lambda = 0.2922 \text{ \AA}$) and the scattered X-rays were detected by a Perkin Elmer XRD1621 (2048x2048 pixels, 200x200um) detector. The diffraction patterns have been measured only along decompression of an amorphous sample obtained from a compression at low temperature while monitoring the changes with Raman spectroscopy. The excellent transverse spatial resolution allows to obtain clean diffraction patterns of the sample without the presence of spurious diffraction lines from the metallic gasket. The empty cell subtraction, which is of fundamental importance to obtain reliable measurements of the diffuse scattering from an amorphous or liquid sample in the DAC, has been in this case easily obtained by measuring the empty cell at the end of the decompression run when the SO_2 has completely back transformed to the gas state and escaped from the sample chamber.

Simulations methodology. We performed a structural search for crystalline phases of SO₂ employing the USPEX (40) package at pressures 10, 20 and 50 GPa with 4 formula units (12 atoms) within unit cell. *Ab initio* simulations were performed by density functional theory (DFT) as implemented in VASP 5.3 and 5.4 codes (41–43), employing projector augmented-wave pseudopotentials (with 6 valence electrons for both S and O atoms) and Perdew-Burke-Ernzerhof (PBE) (44) parametrization of the GGA exchange-correlation functional. In evolutionary search, structural relaxations and enthalpy calculations we employed the harder S_h and O_h pseudopotentials with cutoff of 910 eV while in MD calculations we used the regular ones S and O with cutoff of 520 eV. Compression, decompression and heating were performed by 6 ps variable cell NpT simulations with Langevin thermostat and Γ -point Brillouin zone sampling. We used 10.0 and 2.0 ps⁻¹ friction coefficients for atomic and lattice degrees of freedom respectively, and 10000 *m_u* as barostat fictitious mass. Data for velocity autocorrelation function were generated by equilibrating sample for 6 ps in NpT and then running 20 ps NVE simulation. Total and projected vibrational density of states (VDOS) were computed in standard way as Fourier transform of mass-weighted velocity autocorrelation function from MD trajectories at pressures from 10 to 60 GPa. Static structure factors *S*(*Q*) were calculated by performing Fourier transform of the RDFs from MD trajectories at several pressures along compression and decompression runs.

ACKNOWLEDGMENTS. RM acknowledges stimulating discussions with P. Mach. RM and OT were supported by the Slovak Research and Development Agency under Contract No. APVV-15-0496. Calculations were performed at the Computing Centre of the Slovak Academy of Sciences using the supercomputing infrastructure acquired in ITMS Projects No. 26230120002 and No. 26210120002 (Slovak Infrastructure for High-Performance Computing) supported by the Research and Development Operational Programme funded by the ERDF. Experimental part was supported by the CAS President's International Fellowship Initiative (PIFI), No. 2018VMA0053, and No. 2019VMA0027, National Natural Science Foundation of China (Grant Nos.11874361, 51672279, 11774354 and 51727806), Science Challenge Project (No. TZ2016001), and the CASHIPS Director's Fund (Grant No. YZJJ2017705).

1. PH Poole, TT Grande, CA Angell, PF McMillan, Polymorphic phase transitions in liquids and glasses. *Science* **275**, 322–323 (1997).
2. PF McMillan, Polyamorphic transformations in liquids and glasses. *J. Mater. Chem.* **14**, 1506–1512 (2004).
3. D Machon, F Meersman, M Wilding, M Wilson, P McMillan, Pressure-induced amorphization and polyamorphism: Inorganic and biochemical systems. *Prog. Mater. Sci.* **61**, 216 – 282 (2014).
4. MA Anisimov, et al., Thermodynamics of fluid polyamorphism. *Phys. Rev. X* **8**, 011004 (2018).
5. O Mishima, LD Calvert, E Whalley, 'melting ice' i at 77 k and 10 kbar: a new method of making amorphous solids. *Nature* **310**, 393–395 (1984).
6. O Mishima, LD Calvert, E Whalley, An apparently first-order transition between two amorphous phases of ice induced by pressure. *Nature* **314**, 76–78 (1985).
7. PH Poole, F Sciortino, U Essmann, HE Stanley, Phase behaviour of metastable water. *Nature* **360**, 324–328 (1992).
8. PF McMillan, M Wilson, D Daisenberger, D Machon, A density-driven phase transition between semiconducting and metallic polyamorphs of silicon. *Nature* **4**, 680–684 (2005).
9. M Grimsditch, Polymorphism in Amorphous SiO₂. *Phys. Rev. Lett.* **52**, 2379–2381 (1984).
10. RJ Hemley, AP Jephcoat, HK Mao, LC Ming, MH Manghnani, Pressure-induced amorphization of crystalline silica. *Nature* **334**, 52–54 (1988).
11. Q Williams, R Jeanloz, Spectroscopic evidence for pressure-induced coordination changes in silicate glasses and melts. *Science* **239**, 902–905 (1988).
12. DJ Durben, GH Wolf, Raman spectroscopic study of the pressure-induced coordination change in geO₂ glass. *Phys. Rev. B* **43**, 2355–2363 (1991).
13. C Sanloup, E Gregoryanz, O Degtyareva, M Hanfland, Structural transition in compressed amorphous sulfur. *Phys. Rev. Lett.* **100**, 075701 (2008).
14. L Henry, et al., A density-driven first-order phase transition in liquid sulfur. *arXiv e-prints*, arXiv:1709.09996 (2017).
15. AF Goncharov, E Gregoryanz, H Mao, Z Liu, R Hemley, Optical evidence for a nonmolecular phase of nitrogen above 150 gpa. *Phys. review letters* **85**, 1262–5 (2000).
16. E Gregoryanz, AF Goncharov, R Hemley, H Mao, High-pressure amorphous nitrogen. *Phys. Rev. B* **64** (2001).

17. M Santoro, et al., Amorphous silica-like carbon dioxide. *Nature* **441**, 857–860 (2006).
18. JA Montoya, R Rousseau, M Santoro, F Gorelli, S Scandolo, Mixed threefold and fourfold carbon coordination in compressed CO₂. *Phys. Rev. Lett.* **100**, 163002 (2008).
19. L Ciabini, M Santoro, R Bini, V Schettino, High pressure reactivity of solid benzene probed by infrared spectroscopy. *The J. Chem. Phys.* **116**, 2928–2935 (2002).
20. L Ciabini, M Santoro, R Bini, V Schettino, High pressure photoinduced ring opening of benzene. *Phys. review letters* **88**, 085505 (2002).
21. L Ciabini, et al., Triggering dynamics of the high-pressure benzene amorphization. *Nature* **6**, 39 (2007).
22. C Mailhot, LH Yang, AK McMahan, Polymeric nitrogen. *Phys. Rev. B* **46**, 14419–14435 (1992).
23. MI Eremets, AG Gavriliuk, IA Trojan, DA Dzivenko, R Boehler, Single-bonded cubic form of nitrogen. *Nature* **3**, 558–563 (2004).
24. F Datchi, B Mallick, A Salamat, S Ninet, Structure of polymeric carbon dioxide CO₂–V. *Phys. Rev. Lett.* **108**, 125701 (2012).
25. M Santoro, et al., Partially collapsed cristobalite structure in the non molecular phase v in CO₂. *Proc. Natl. Acad. Sci.* **109**, 5176–5179 (2012).
26. JE House, *Inorganic Chemistry*. (Academic Press), (2008).
27. TY Takeshita, BA Lindquist, TH Dunning, Insights into the electronic structure of ozone and sulfur dioxide from generalized valence bond theory: Bonding in O₃ and SO₂. *The J. Phys. Chem. A* **119**, 7683–7694 (2015) PMID: 26068052.
28. Y Song, Z Liu, H Mao, RJ Hemley, DR Herschbach, High-pressure vibrational spectroscopy of sulfur dioxide. *The J. Chem. Phys.* **122**, 174511 (2005).
29. M Ceppatelli, M Santoro, R Bini, V Schettino, High pressure reactivity of solid furan probed by infrared and raman spectroscopy. *The J. Chem. Phys.* **118**, 1499–1506 (2003).
30. M Santoro, M Ceppatelli, R Bini, V Schettino, High-pressure photochemistry of furane crystal. *The J. Chem. Phys.* **118**, 8321–8325 (2003).
31. JH Eggert, G Weck, P Loubeyre, M Mezouar, Quantitative structure factor and density measurements of high-pressure fluids in diamond anvil cells by x-ray diffraction: Argon and water. *Phys. Rev. B* **65**, 174105 (2002).
32. B Post, RS Schwartz, I Fankuchen, The crystal structure of sulfur dioxide. *Acta Crystallogr.* **5**, 372–374 (1952).
33. Kenny, Stahl, The crystal structure of SeO₂ at 139 and 286 K. *Zeitschrift fUMLAUT@ur Kristallographie - Crystalline Materials* **202**, 99–108 (1994).
34. C Groves, E Lewars, Dimers, trimers and oligomers of sulfur oxides: an ab initio and density functional study. *J. Mol. Struct. THEOCHEM* **530**, 265 – 279 (2000).
35. G Frapper, Polysulfite, a hypothetical allotrope of sulfur dioxide? a molecular and periodic quantum investigation of covalent oligomeric and one-dimensional SO₂-based compounds (x = s, se). *New J. Chem.* **25**, 440–445 (2001).
36. R Wentorf, Chemistry at high pressures, the physics and chemistry of high pressure. *Soc. Chem. Ind. London, S.W.* **1**, 185 – 190 (1963).
37. Neuhaus, A., Synthese, Strukturverhalten und Valenzzustande der anorganischen Materie im Bereich hoher und hochster Drucke. *Chimia* **18**, 93–103 (1964).
38. CT Prewitt, RT Down, High-pressure crystal chemistry. *Rev. Miner.* **37**, 283–317 (1998).
39. TA Manz, NG Limas, Introducing ddec6 atomic population analysis: part 1. charge partitioning theory and methodology. *RSC Adv.* **6**, 47771–47801 (2016).
40. C Glass, A Oganov, N Hansen, Uspex - evolutionary crystal structure prediction. *Comp. Phys. Comm.* **175**, 713–720 (2006).
41. G Kresse, GJ Hafner, *Ab initio* molecular dynamics for liquid metals. *Phys. Rev. B* **47**, 558–561 (1993).
42. G Kresse, J Furthmuller, Efficiency of ab-initio total energy calculations for metals and semiconductors using a plane-wave basis set. *Comput. Mater. Sci.* **6**, 15 – 50 (1996).
43. G Kresse, J Furthmuller, Efficient iterative schemes for ab initio total-energy calculations using a plane-wave basis set. *Phys. Rev. B* **54**, 11169–11186 (1996).
44. JP Perdew, K Burke, M Ernzerhof, Generalized gradient approximation made simple. *Phys. Rev. Lett.* **77**, 3865–3868 (1996).